Volume 54
Number 34
14 September 2025
Pages 12703-12988

Dalton Transactions

An international journal of inorganic chemistry

rsc.li/dalton

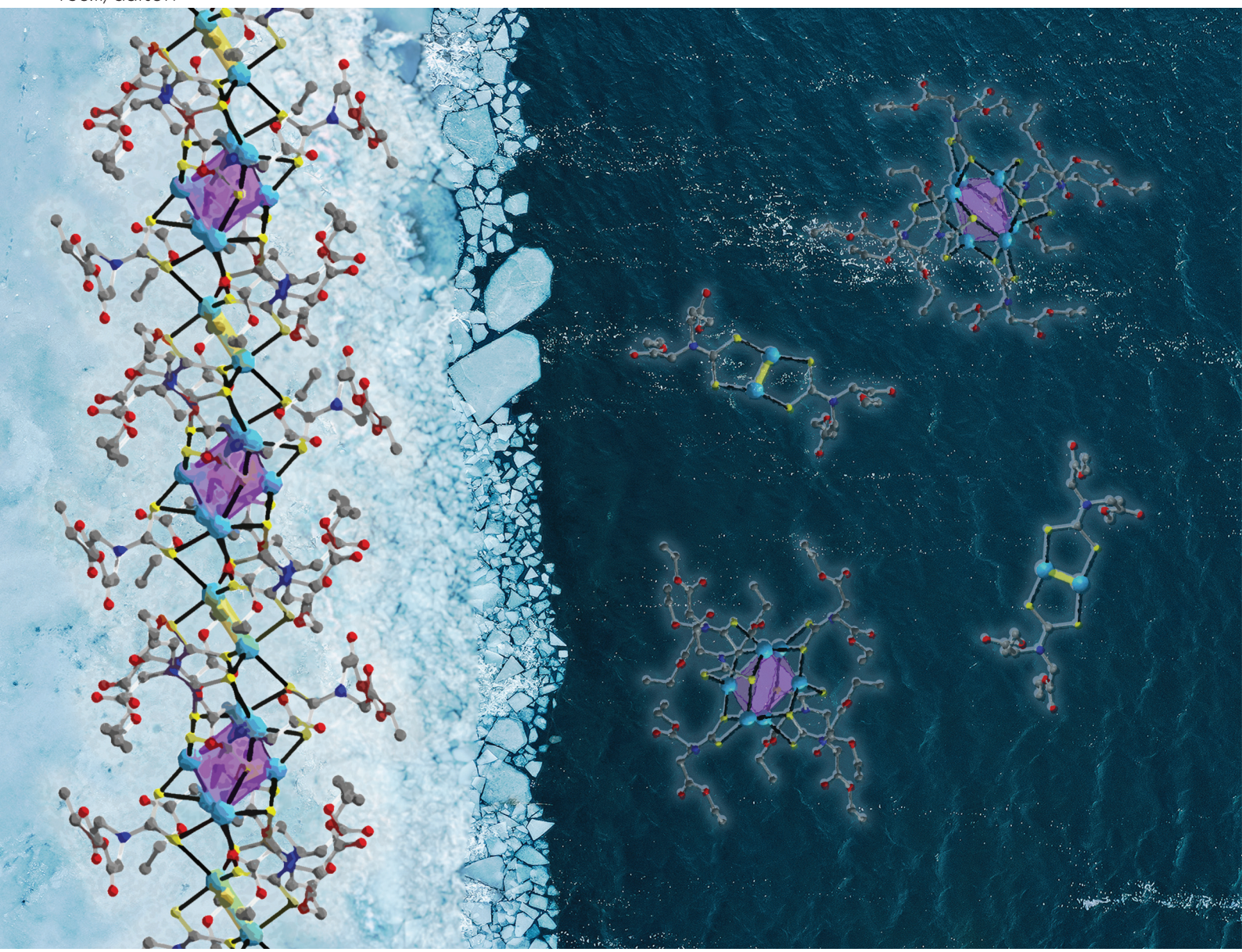

ISSN 1477-9226

ROYAL SOCIETY OF CHEMISTRY

PAPER
Phil Köhler *et al.*
Silver dithiocarbamates derived from amino acid esters

Dalton Transactions

ROYAL SOCIETY OF CHEMISTRY

PAPER

View Article Online
View Journal | View Issue

Cite this: *Dalton Trans.*, 2025, **54**, 12772

Silver dithiocarbamates derived from amino acid esters

Vreni Behling, [a] Jakob Heinrich,[a] Dolores Díaz,[b] Elias H. P. Brohmer,[c] Julian Heinrich,[d] Nils Schlörer,[b] Stephan Kupfer, [c] Nora Kulak [d] and Phil Köhler *[a]

Received 23rd June 2025,
Accepted 1st August 2025

DOI: 10.1039/d5dt01476j

rsc.li/dalton

We report herein a series of new silver compounds with dithiocarbamate ligands derived from amino acid esters (AAE-DTCs). Compounds $[Ag\{SSC\text{-}N(R')(CH_2R''COOR)\}]_n$ (**Ag(L1)–Ag(L5)**; *N*-dithioato-diethyl-iminodiacetate (**L1**), -ethyl-sarcosinate (**L2**), -*tert*-butyl-sarcosinate (**L3**), -methyl-L-prolinate (**L4**), -ethyl-*N*-benzylglycinate (**L5**)) were synthesised from *in situ* generated AAE-DTCs by salt metathesis with silver nitrate. The isolated products were characterised by different analytical techniques. **Ag(L1)**, **Ag(L4)**, and **Ag(L5)** were accessible to single-crystal X-ray structure determination, comprising hexameric subunits linked by dimeric units into a 1D-polymeric structure (**Ag(L1)**) and more homogeneous ribbon-like polymeric structures (**Ag(L4)** and **Ag(L5)**). DOSY NMR measurements and supporting DFT calculations were carried out to elucidate the structure of these compounds in solution, showing evidence for smaller agglomerates like dimers and tetramers. Additionally, as first evaluation of the biological activity of these complexes, ethidium bromide displacement assays and DNA melting curve experiments were carried out, the results showing moderate DNA binding abilities.

Introduction

Dithiocarbamate ligands derived from amino acids (AA-DTCs) and their transition metal complexes have been widely investigated. While these compounds function as ditopic S,O-ligands in the synthesis of heterobimetallic coordination compounds,[1] they have attracted particular attention for various applications in biological systems. Investigations were carried out for example on manganese complexes of the type $[Mn(AA\text{-}DTC)(CO)_4]$ as CO-releasing molecules,[2–5] on technetium complexes of the type $[TcN(AA\text{-}DTC)_2]$ as radiopharmaceuticals,[6–8] on iron(III) complexes of the type $[Fe(AA\text{-}DTC)_3]$ and related species as NO spin traps for EPR imaging,[9–13] and on copper(II) complexes of the type $[Cu(AA\text{-}DTC)_2]$ for various applications because of their redox activity.[14–17] Late transition metal derivatives of the 4d and 5d series have been investigated as anticancer agents. These include palladium and platinum complexes of the type $[M(AA\text{-}DTC)_2]$ (M = Pd, Pt) and related heteroleptic complexes,[18–26] gold(III) complexes of the type $[AuX_2(AA\text{-}DTC)]$ (X = Br, Cl),[21,22,27–33] and ruthenium(III) complexes of the type $[Ru(AA\text{-}DTC)_3]$.[14,34,35]

Silver compounds have been of great interest regarding their biological activity. Silver nanoparticles are already in use in several biomedical applications[36] and many silver coordination compounds are being evaluated for their clinical potential because of antibacterial, anti-inflammatory, and antiseptic properties, as well as their potential in overcoming drug resistance in bacteria.[37] Comparable research on silver AA-DTCs has, to the best of our knowledge, not been reported. Nevertheless, silver is long known to also form complexes with DTC ligands,[38] although the homoleptic products are not discrete mononuclear entities like for many other late-transition metal ions, but instead form oligo- and polynuclear assemblies, that can also be found for the other monovalent coinage metals.[38] While Au(I)-DTC compounds usually form dimers, sometimes further connected to polymeric chains by aurophilic contacts, and literature data on Cu(I)-DTC compounds suggest the preference of tetrameric assemblies, structure elucidation of homoleptic Ag(I) DTCs by X-ray diffraction showcases that these oligo- or polynuclear compounds exist as cage-like oligomeric molecules[39–43] or polymeric chains[43–48] in the solid state. Heteroleptic Ag-DTC compounds with phosphine ligands on the other hand have been shown to form discrete mononuclear,[49–52] dinuclear[52–54] or polynuclear assemblies[52,55] depending on the nature of the additional

[a]*Institute of Inorganic and Analytical Chemistry, Friedrich Schiller University Jena, Humboldtstr. 8, 07743 Jena, Germany. E-mail: phil.koehler@uni-jena.de*
[b]*NMR platform, Friedrich Schiller University Jena, Humboldtstr. 10, 07743 Jena, Germany*
[c]*Institute of Physical Chemistry, Friedrich Schiller University Jena, Helmholtzweg 4, 07743 Jena, Germany*
[d]*Institute of Chemistry, University Potsdam, Karl-Liebknecht-Str. 24-25, 14476 Potsdam, Germany*

ligands. The Ag compounds have been synthesised by salt metathesis from DTC ligands and a suitable Ag salt like $AgNO_3$ [42,43,47,48,50,51,53,54,56–60] or $AgClO_4$.[55] Homoleptic Ag-DTC compounds have been investigated as single-source precursors for silver sulphide nanoparticles[50,56] while some heteroleptic compounds have been explored regarding their biological activity, specifically an antibacterial activity especially against Gram-positive bacteria has been found.[51,54] But it is noteworthy that so far in most cases only non-functionalised DTC ligands were used in the syntheses of Ag complexes in contrast to the AA-DTCs used in the previously mentioned biologically active complexes with different transition metals.

Our studies focus on Ag complexes with DTC ligands derived from α-aminocarboxylic acid esters (AAE-DTCs). As detailed above, metal complexes with AAE-DTCs often exhibit high biological activity and the hydrophobic ester groups exert a striking influence on their biodistribution.[8,14,17–21,24–28,30–32,34,61–65] Some reports discuss potential negative effects of free carboxylate groups on the stability and/or biological activity of the metal AA-DTCs. There is evidence for the improvement of the biological activity by esterification in some systems.[28,64] We report herein the synthesis and characterisation of a series of Ag(I) complexes with AAE-DTC ligands derived from esters of iminodiacetic acid, sarcosine, L-proline, and benzyl glycine (see Fig. 1). This includes solid state structure determination by single-crystal X-ray diffraction (SC-XRD) and DOSY NMR measurements to gain insight into the aggregation in solution, DFT calculations, as well as DNA binding studies.

Results and discussion

Synthesis and general characterisation

It is known that DTCs and their respective complexes formed from primary amines are less stable than those formed from secondary amines.[38] That holds true as well for Ag DTC complexes as investigated in this study. While analytically pure target products could be isolated as white or yellow solids for secondary AAE derivatives as described below, the same cannot be observed for primary AAEs. Instead undefined dark precipitates are obtained under the same reaction conditions for derivatives of primary AAEs *e.g.* glycine methyl ester and L-alanine methyl ester. To avoid cleavage of the ester groups because of overly alkaline conditions, our established reaction procedure was adapted according to a literature procedure[32] with an additional equivalent of the amino acid ester acting as the base, thus producing the respective AAE hydronitrate as byproduct. A solution of $AgNO_3$ was directly added to the *in situ* generated dithiocarbamate, causing formation of a pale yellow precipitate, that could be isolated and characterised (Scheme 1). Following this procedure, silver complexes **Ag(L1)**, **Ag(L2)**, **Ag(L3)** and **Ag(L4)** could be isolated from aqueous solution. Because of the different solubility of benzyl glycine derived ligands the synthesis of **Ag(L5)** was carried out in a MeOH/DMSO mixture. The product could be crystallised directly from the reaction solution by layering it with MeOH.

The isolated compounds were characterised by elemental analyses (C, H, N), IR spectroscopy, thermal analyses (TGA) and solution NMR spectroscopy where applicable. Except for **Ag(L2)** the isolated products were adequately soluble in either DMSO-d_6 or chloroform-*d* to measure ^{1}H and ^{13}C NMR spectra. The isolated yields as well as the temperatures of decomposition (T_{dec}) and selected IR bands are listed in Table 1. The IR spectra show the expected ν(C=O) bands for a carboxylic ester between 1721 and 1740 cm^{-1}, which is at slightly higher wavenumbers than the bands would be expected for carboxylic acids and significantly higher than the expected value for free carboxylates.[66] These band positions show that the ester groups stayed intact throughout the syntheses and do most likely not contribute significantly to metal coordination. The ^{1}H and ^{13}C NMR spectra also show the intact ester groups, with the COOR signals between 166.5 and 171.2 ppm observed at slightly higher fields compared to the expectation for COOH and more significantly compared to COO^-.[67] The ν(C–N) bands observed between 1414–1476 cm^{-1} are between the ranges for stretching vibrations of single (C–N) and double bonds (C=N) and therefore indicate a partial C–N double bond character of the dithiocarbamate moiety. For four of the five compounds the ν(C–N) bands are at very similar wavenumbers, only for **Ag(L4)** it is found at a slightly lower wavenumber. This range agrees with values found for other published Ag DTC compounds.[49,55–57] Values found for complexes with the other monovalent coinage metals are at the upper end of this range (1481 cm^{-1} for $[Au(L2)]_2$ [32] and 1478–1500 cm^{-1} for Cu(I) DTCs[68]). For divalent $[M(DTC)_2]$

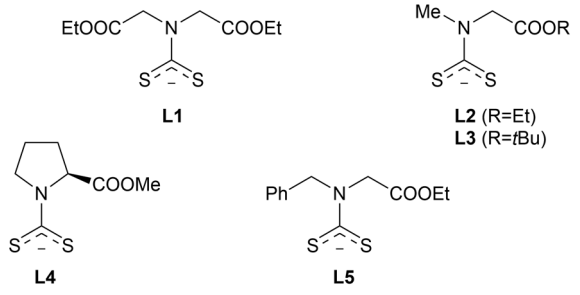

Fig. 1 AAE-DTC ligands used in this work.

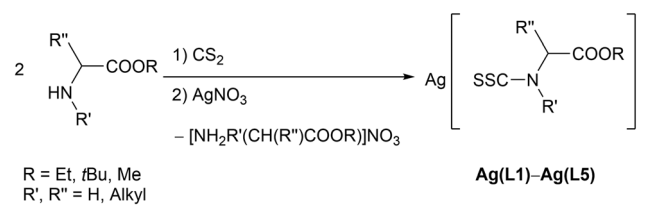

Scheme 1 Synthesis of Ag-AAE-DTC complexes **Ag(L1)**, **Ag(L2)**, **Ag(L3)**, **Ag(L4)** and **Ag(L5)** starting from iminodiacetic acid diethyl ester, sarcosine ethyl ester, sarcosine *tert*-butyl ester, L-proline methyl ester and *N*-benzyl glycine ethyl ester.

Table 1 Isolated yields (not optimised), temperatures of decomposition (T_{dec}), selected IR band positions and NMR shifts for the Ag-AAE-DTC compounds (R = Et, *t*Bu, Me)

Compound	Yield [%]	T_{dec} [°C]	ν(C=O) [cm^{-1}]	ν(C–N) [cm^{-1}]	δ (CSS) [ppm]	δ (COOR) [ppm]
Ag(L1)	78	227	1721	1466	208.4	167.3
Ag(L2)	99	236	1730	1470	—[a]	—[a]
Ag(L3)	98	199	1734	1476	207.9	166.5
Ag(L4)	99	240	1740, 1730	1414	203.2	171.2
Ag(L5)	93	252	1734	1454	208.4	167.4

[a] No NMR spectra obtained, due to the insolubility of the compound.

complexes (M = Ni, Pd, Pt, Cu, Zn) this band is expected at slightly higher wavenumbers due to the higher charge and resulting stronger C–N double bond character. Reported values match this expectation.[17,69,70] TGA measurements under nitrogen give decomposition temperatures between 199 and 252 °C which is in the same range as previously reported for unsubstituted Ag DTCs.[49,50,53,55,57–60,71] The observed T_{dec} values do not follow any clear trend, neither regarding the substitution pattern of the amino acid scaffold, nor in comparison with AAE-DTC complexes of other metal ions. For instance, for homoleptic complexes of **L2** and **L3** with Ru(III),[34] Ni(II),[69] and Au(I)[32] slightly lower decomposition temperatures have been reported, while complexes of Cu(II),[17] Zn(II),[70] and Pt(II)[69] show decomposition in a similar temperature range.

Solid-state molecular structures

Single crystals suitable for X-ray structural analysis of compound **Ag(L1)** were obtained from water/ethanol (space group $P\bar{1}$). The asymmetric unit contains four [Ag(L)] units. The four different dithiocarbamate groups display two different coordination modes (*vide infra*). The connection of Ag and S atoms results in a one-dimensional polymeric structure (see Fig. 2) best described as an assembly of alternating dimeric and hexameric subunits (both centrosymmetric). The dimeric subunit consists of two Ag atoms (Ag3 and a symmetry equivalent) that are connected by two bridging ligand moieties. For the hexameric subunit, two six-membered metallacycles [Ag_3S_3] in a chair-like conformation of alternating Ag and S atoms (one S atom of each DTC unit) are stacked on top of each other. The two S atoms of the DTC moieties differ in their coordination. S1, S6, S7 and their symmetry equivalents each link two Ag atoms and thus form the six-membered metallacycles, while the second S atom of each DTC unit (S2, S5, S8, and their symmetry equivalents) connects the two rings by coordinating to one Ag atom of the other metallacycle. The six Ag atoms form a distorted octahedron similar to the structure shown in Fig. 5d (CSD ref. code WIHNEH).[42] Unlike this previously published structure, where discrete hexamers were formed, an additional Ag–S bond (S2–Ag3 259.48(3) pm) connects the hexameric and the dimeric subunit, thus creating a polymeric structure. Additionally, there are two longer Ag–S contacts (Ag1–S3 290.36 (5) and Ag3–S5 300.47(4) pm) between the subunits.

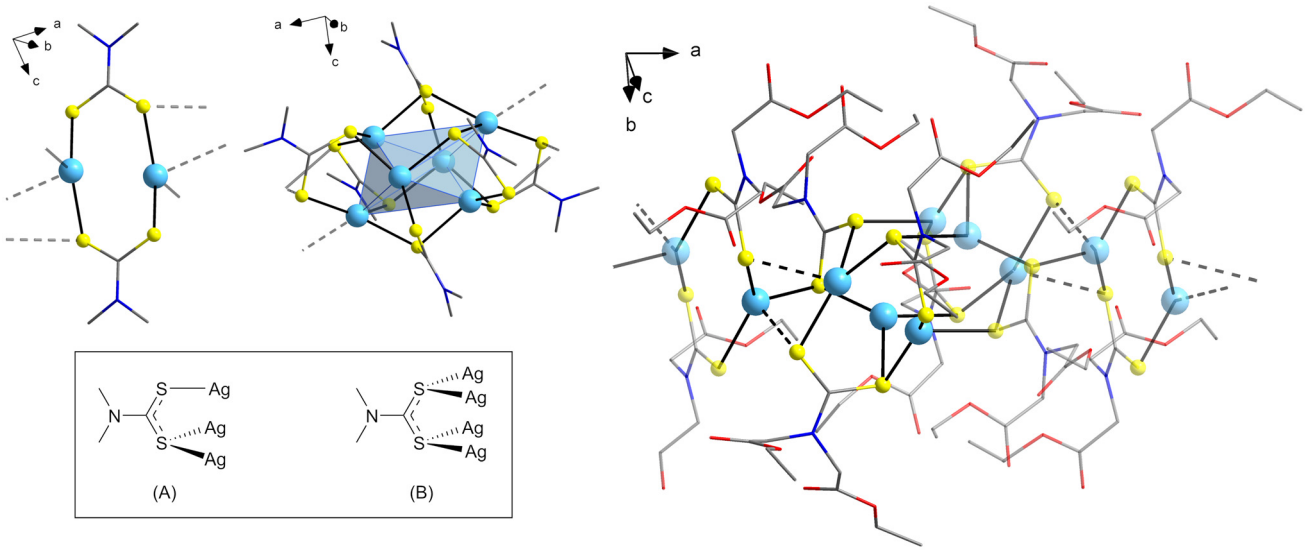

Fig. 2 Dimeric subunit, hexameric subunit and extract of the polymeric structure in the crystals of **Ag(L1)**, extending in *a*-axis direction. The ligand moieties are drawn in a wire model for clarity. Ag–S bonds between 245–265 pm are drawn with a solid line, while longer Ag–S bonds (290–305 pm) are drawn as a dashed line (Ag = light blue, S = yellow, O = red, N = blue, C = grey). Framed entry: coordination modes of the dithiocarbamate group in **Ag(L1)** considering both the short and the long Ag–S contacts: (A) κS:κS:κS′, (B) κS:κS:κS′:κS′.

Single crystals suitable for X-ray diffraction of compound **Ag(L4)** were obtained from a solution in DMSO (space group *P*1). The unit cell contains eight [Ag(L)] units being part of two polymeric chains. The two entities are structurally very similar and vary mostly in the position of one of the S atoms (S2/S10) and the more flexible ligand residues, as can be seen in the overlay of both strands in Fig. 3. All four dithiocarbamate groups in one strand display different coordination modes (*vide infra*). The connection of Ag and S atoms results in a one-dimensional ribbon-like polymeric structure (Fig. 4) with no direct Ag···O contacts.

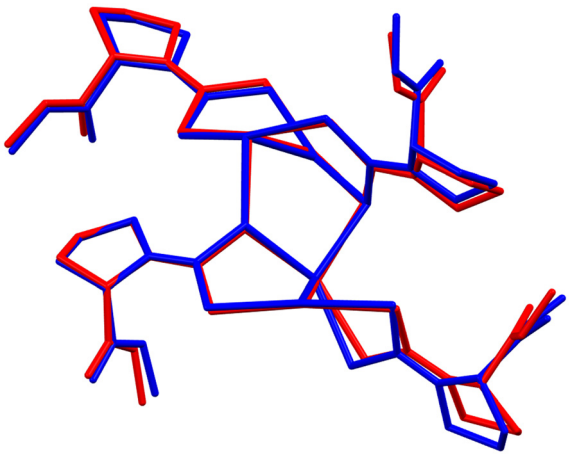

Fig. 3 Molecule overlay of the two tetranuclear fragments within the asymmetric unit from the crystal structure of **Ag(L4)**, illustrating the slight differences in both strands. The strand containing Ag1 is red, that containing Ag5 is blue.

Compound **Ag(L5)** crystallises in space group *Pbca* with two [Ag(L)] units in the asymmetric unit. Both dithiocarbamate groups display different coordination modes (*vide infra*). The linkage between Ag atoms and S donors results in the formation of a one-dimensional polymeric structure with no direct Ag···O contacts, similar to that of **Ag(L4)**.

The bond lengths within the dithiocarbamate moieties in all three structures suggest a considerable double bond character for the C–N bond within the DTC functional group. The C–N bond lengths range from 132.97(2)–135.52(2) pm, 132(2)–134(2) pm, and 134.28(1)–134.79(0) pm for **Ag(L1)**, **Ag(L4)**, and **Ag(L5)**, respectively, while the other C–N bonds of the dithiocarbamate moieties are in the range from 145.09(3)–146.51(2) pm, 147(2)–150(2) pm, and 144.68(1)–147.29(1) pm. These values fit previously reported C–N bond lengths.[72] The longer C–N bonds in the structure of **Ag(L4)** agree with the observed IR band positions. The Ag–S bond lengths are in the range 249.25(4)–262.51(5) pm with two longer bonds (290.36(5) and 300.47(4) pm) for **Ag(L1)**, 240.5(4)–303.3(4) pm for **Ag(L4)**, and 249.57(1)–274.71(2) pm for **Ag(L5)**, which is in agreement with the range observed for other Ag(I) DTCs deposited in the Cambridge Structural Database (CSD).[73] Of the four Ag atoms in the asymmetric unit of **Ag(L1)**, two Ag atoms (Ag2/Ag4) are coordinated by three S atoms belonging to three different ligand moieties each, while the other two (Ag1/Ag3) are coordinated by four S atoms belonging to four different ligand moieties each. Since one of those four bonds is significantly longer than the other three, it can be considered as a [3 + 1]

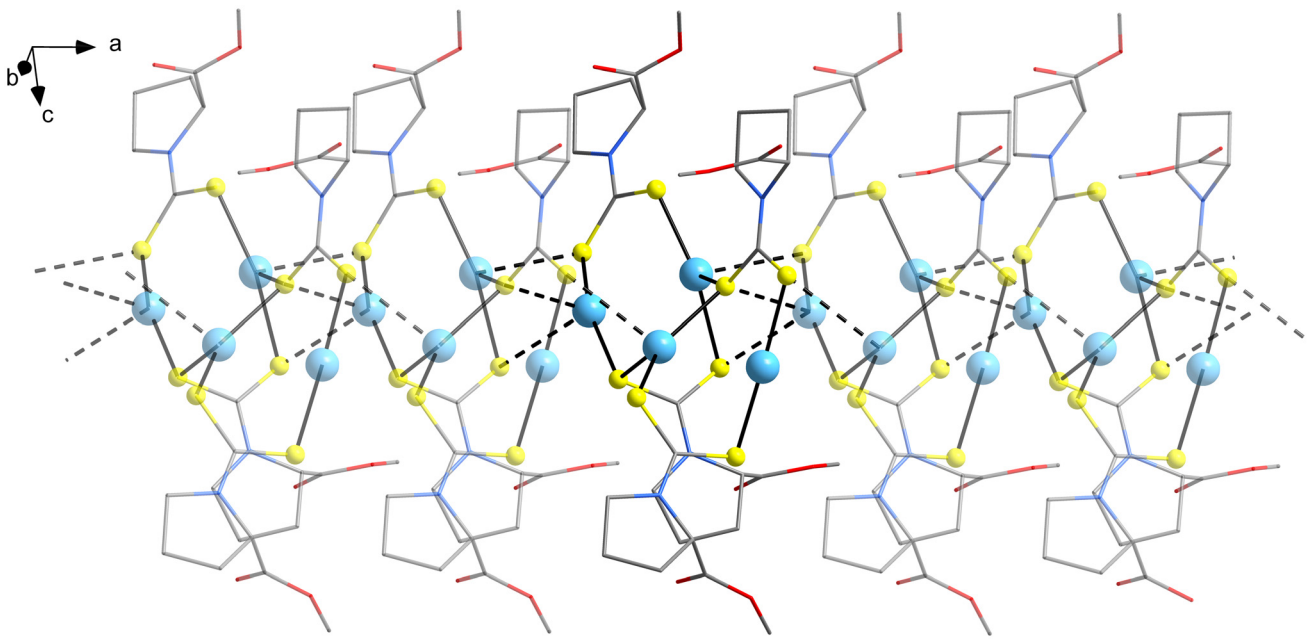

Fig. 4 Extract of the ribbon-like polymeric structure in the crystals of **Ag(L4)**, extending in *a*-axis direction. The ligand moieties are drawn in a wire model for clarity. Ag–S bonds between 240–270 pm are drawn with a solid line, while longer Ag–S bonds (280–305 pm) are drawn as a dashed line (Ag = light blue, S = yellow, O = red, N = blue, C = grey).

coordination. Geometrical analysis[74] shows a close resemblance to a vacant tetrahedron for the two three-coordinated Ag atoms Ag2 and Ag4. For Ag1 and Ag3 the SHAPE parameters for polyhedra of coordination number 3 (excluding the longer Ag–S bond) and 4 (including the longer Ag–S bond) have been calculated (Table S6). The results show a very good agreement with a trigonal coordination for the short Ag–S bonds of Ag3, indicating only a weak interaction for the longer Ag···S contact. For Ag1 the distortion from an ideal trigonal shape is larger, suggesting that the impact of the additional Ag···S contact might be stronger. In the structure of **Ag(L4)** in each of the chains one of the four different Ag atoms (Ag1/Ag5) is coordinated by two S atoms in an almost linear fashion, the S–Ag–S angles being 172.6(1)° and 172.7(1)°, respectively. The other three Ag atoms in a chain are coordinated by four S atoms belonging to four different ligand moieties each. Geometrical analysis shows significant deviation from an ideal tetrahedral coordination. The closest to ideal tetrahedral coordination are Ag2 and Ag6, respectively. For Ag3/Ag7 and Ag4/Ag8 there are two short (242.2(4)–249.1(4) pm) and two longer Ag–S bonds (275.9(4)–296.5(4) pm) per Ag atom, accounting for a larger deviation from the ideal tetrahedron. In the structure of **Ag(L5)** both Ag atoms are coordinated by four S atoms from four ligand molecules, respectively. Geometrical analysis shows a significant deviation from the ideal tetrahedral geometry for both Ag centres, with Ag1 being less distorted (Table S6). The highly diverse metal–ligand connectivity in the title compounds also reflects in the observed coordination patterns of the DTC ligating groups, comprising various highly bridging modes. In all three structures, the symmetric coordination mode κS:κS:κS′:κS′ is present, as well as the less symmetric κS:κS:κS′ mode in the structures of **Ag(L1)** and **Ag(L4)**. The DTC ligands in **Ag(L4)** additionally show coordination modes κS:κS′ and κS:κS:κS:κS′:κS′, while κS:κS:κS:κS′ is present in the structure of **Ag(L5)**. Such coordination modes are very typical for lowly charged metal cations such as the monovalent coinage metals, which can be explained by the relatively weak electrostatic repulsion between the metal centres on the one hand, and by potential metallophilic attractions on the other hand.[38]

Molecular structures in solution

While for Ag DTCs the existence of oligo- or polymeric structures in the solid state are well substantiated (see Introduction), little is known about their structures in solution. It has been theorized that disaggregation to smaller agglomerates can take place upon dissolution.[38,39] Possible oligomers with exemplary structural motifs as found in the crystalline state are shown in Fig. 5. To ascertain the structure and molecular size of the title compounds in solution, their

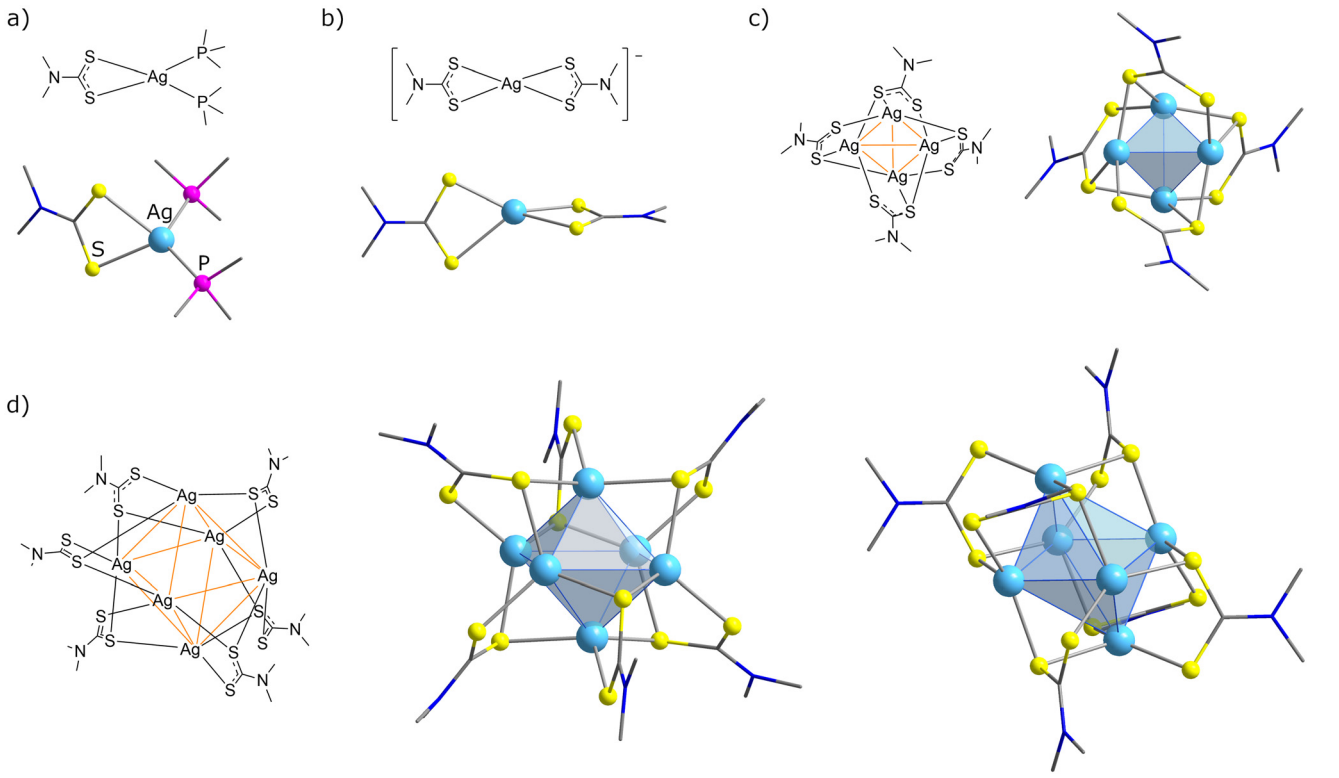

Fig. 5 Possible oligomers for Ag-DTCs as investigated with DOSY NMR and DFT calculations. Exemplary structural motifs found for the respective oligomers for silver(I) dithiocarbamates in the crystalline state are given (N = blue, C = grey) (the ref. codes of the respective entries in the Cambridge Structural Database (CSD)[73] are given in parentheses): (a) heteroleptic monomer (DUBBEJ), (b) anionic $[Ag(DTC)_2]^-$ complex (HEVGIC), (c) tetramer with the silver atoms on the corners of a tetrahedron (JOLJIH), (d) hexamer with the silver atoms on the corners of a rather regular octahedron (QIBJIY), and a significantly distorted octahedron (WIHNEH); the transition between the two hexameric forms is fluent.

Table 2 Diffusion coefficients calculated from DOSY experiments and predicted agglomeration (n) of the species in solution

Compound	Solvent	D^a [10^{-10} m^2 s^{-1}]	n
Ag(L1)	DMSO-d_6	1.01	2
Ag(L3)	$CDCl_3$	3.79	≥4
Ag(L4)	$CDCl_3$	3.84	≥4
Ag(L5)	$CDCl_3$	3.79	≥4
Ag(L5)	DMSO-d_6	1.02	2

[a] Experimental diffusion coefficient calculated with relaxation module from TopSpin (Bruker).

diffusion coefficients were measured using DOSY NMR (Table 2 and Tables S1, S2, Fig. S9). Depending on their solubility, samples were prepared in either DMSO-d_6 or $CDCl_3$. The diffusion coefficients D of **Ag(L1)** and **Ag(L5)** in DMSO-d_6 were nearly identical, suggesting similar structures in solution. Almost the same occurred with compounds **Ag(L3)**, **Ag(L4)**, and **Ag(L5)** in $CDCl_3$, although the differences between D values were larger than in DMSO-d_6 possibly as consequence of the intrinsic differences in molecular weight of the monomeric units for the samples dissolved in $CDCl_3$. Internal diffusion references with a known molecular weight can be used to semiquantitatively estimate the molecular weight of a substance from its D value.[75] Thus, to correlate the experimental D values of the Ag(AAE-DTC) compounds with their molecular weight, we have performed additional DOSY measurements of selected Ag(AAE-DTC) samples in DMSO-d_6 or $CDCl_3$ containing also internal diffusion reference compounds. In Fig. S9(a), the 2D DOSY spectrum of a **Ag(L1)** sample in DMSO-d_6 containing sucrose and a short peptide as internal diffusion references shows that the apparent molecular weight of **Ag(L1)** must be between those of the references and would fit with a dimer (see D values in Table 2). For samples dissolved in $CDCl_3$, we followed the same approach and found that the diffusion coefficients were smaller than those of the internal references, suggesting that the molecular weights of those compounds are at least in the range of the corresponding tetramers. Interestingly, the data of the only system investigated in both solvents, **Ag(L5)**, shows that intermolecular interactions with the solvent may play a role and stabilize different oligomeric Ag(AAE-DTC) species in solution. These findings suggest that smaller agglomerates are formed in a coordinating solvent like DMSO as compared to a non-coordinating solvent like chloroform.

The disaggregation of the coordination polymers to different oligomers in solution was further substantiated by ESI mass spectrometry, showing different oligonuclear agglomerates for compounds **Ag(L1)**, **Ag(L3)** and **Ag(L4)**. Peaks can be assigned to $[Ag_nL_{n-1}]^+$ (n = 4, 5, 6). For **Ag(L4)** additionally $[Ag_7L_6]^+$ can be assigned. In all three cases the base peak corresponds to the fragment with n = 6, which formally corresponds to hexamers after the loss of one AAE-DTC ligand. Tendency toward the formation of hexanuclear assemblies (see Fig. 5(d)) is well-documented for Ag DTCs in the literature.[39,41–43] In the mass spectrum of **Ag(L5)** less agglomerates are visible. Instead the base peak corresponds to the free amino acid ester and only a very weak peak set for the agglomerate with n = 6 can be observed. A very weak peak of the respective amino acid ester can also be found in the spectrum of **Ag(L1)**.

DFT calculations

In order to assess the formation of oligomeric species as inferred from the DOSY NMR data further and to elucidate the underlying thermodynamic properties, we performed a computational modelling study on several aggregates of **Ag(L2)** (see Fig. 6). These quantum chemical simulations (see Computational details) were performed in chloroform and acetonitrile as representative examples of non-coordinating and coordinating solvents, respectively. A dimeric complex with linearly coordinated Ag atoms (similar to respective Au(I) complexes) was set at 0 kJ mol^{-1} to be taken as reference point. The energies resulting from the calculations show the tendency in both solvents that larger agglomerates are thermodynamically more stable. In both solvents the tetramer is favoured among the investigated oligomers with a stabilisation energy with respect to the reference system of −77.79 kJ mol^{-1} in acetonitrile and −76.95 kJ mol^{-1} in chloroform. Notable, fully optimised equilibrium structures for larger oligomers, *i.e.*

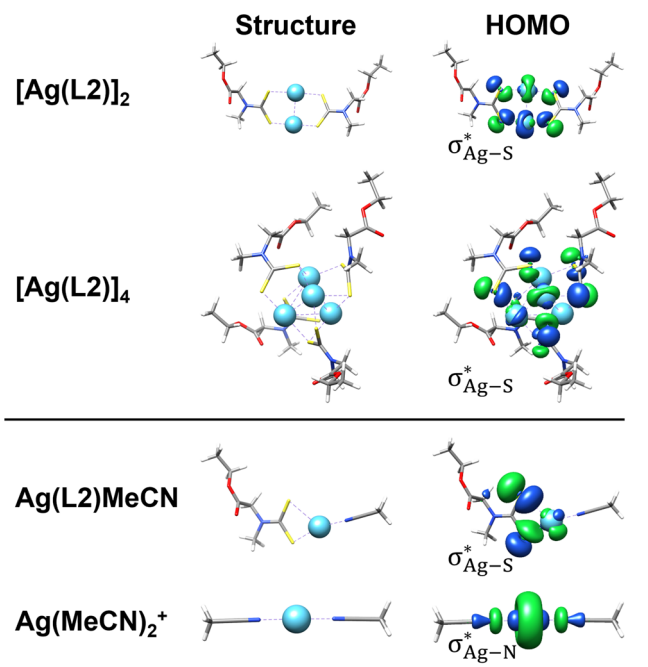

Fig. 6 Fully optimised equilibrium structures as well as highest occupied molecular orbital (HOMO) of $[Ag(L2)]_2$ and $[Ag(L2)]_4$ as well as conceivable solvated species [Ag(L2)MeCN] and $[Ag(MeCN)_2]^+$ (Ag = light blue, S = yellow, O = red, N = blue, C = grey, H = white). Calculations for $[Ag(L2)]_2$ and $[Ag(L2)]_4$ were performed with an implicit solvent environment (acetonitrile); in case of [Ag(L2)MeCN] and $[Ag(MeCN)_2]^+$ a microsolvation model was utilised. All fully relaxed structures are freely available *via* the online repository Zenodo.[76]

with n = 6, could not be obtained. Reactions to smaller complexes where acetonitrile coordinates with the monomer, [Ag(L2)MeCN], are predicted to be thermodynamically less favourable (83.08 kJ mol^{-1}, see Table S3). Furthermore, the formation of an ion pair comprising of $[Ag(MeCN)_2]^+$ and $[Ag(L2)_2]^-$ was considered with the computational approach. Likewise, the formation of such an ion pair is theoretically unfavourable (75.35 kJ mol^{-1}) with respect to the dimer structure (0 kJ mol^{-1}, reference). Therefore, our DFT simulations strongly indicate that the formation of rather large **Ag(L2)** oligomers is thermodynamically favoured. Furthermore, we explored the electronic structures of the different theoretical molecules. The HOMOs are given by the σ_{Ag-S}* orbitals formed by the d(Ag) and p(S) orbitals (see Fig. 6), corroborating the picture that the $[Ag(DTC)]_n$ core represents the most reactive part of the molecule.

DNA binding ability

As initial biological evaluation of the title compounds, their interaction with DNA was studied using ethidium bromide (EB) displacement assays and DNA melting curve experiments. From the EB displacement assays it could be concluded, that the K_{app} values of all complexes are in the same order of magnitude (see Table 3) and hint to electrostatic and/or groove binding interactions towards DNA (K_{app} <10^6 M^{-1}).[77–79] Overall, the DNA binding abilities of the complexes can be considered as moderate. The K_{app} values are an order of magnitude smaller than values published for Au(III), Pd(II), and Zn(II) DTC complexes,[22] which seems reasonable considering the higher oxidation numbers of these metal centres. For $AgNO_3$, the K_{app} value indicates a partial intercalation binding mode, which can be excluded since the Ag^+ cation has no binding ligand with such an intercalative group. Thus, in this case the positive charge of the "unshielded" (solvated) metal cation dominates and interacts with the negatively charged CT-DNA in an enhanced manner in comparison to the complexes, so that EB is displaced efficiently. Furthermore, the fact that $AgNO_3$ has a K_{app} value one order of magnitude higher than the values of the complexes is an indication that the complexes are stable under these experimental conditions (pH 7.4, 2% DMSO in H_2O).

In general, in the DNA melting experiments the same results were obtained as in the EB displacement assay (except for **Ag(L4)**, *vide infra* for explanation). **Ag(L5)** shows a moderate DNA interaction with ΔT_m = 0.1 °C, which hints to electrostatic and/or groove binding. Furthermore, $AgNO_3$ has the strongest DNA binding ability with a T_m shift of 9.1 °C, which is unprecedented for a "naked" metal cation such as Ag^+. A very strong electrostatic interaction of Ag^+ towards DNA and/or even tight nucleobase binding[80–83] is likely causing such strong stabilisation of DNA (condensation) as also described in the EB displacement assay. For **Ag(L4)** an unusual DNA melting curve progression is observed (see Fig. S15). The DNA melting curves can thus not be evaluated. It seems that at higher temperature (>78 °C) the melted single strands are reconnected (drop in absorption intensity above 78 °C). This might be caused by a dissociation of the ligands under heat in a way that afterwards uncoordinated Ag^+ binds strongly/efficiently to DNA (as found in EB displacement assay and DNA melting curves experiments). Thus, this Ag^+ cation binding leads to stabilization of the double helix causing its formation at higher temperatures (DNA condensation).[83,84] Consequently, the absorption intensity drops at 260 nm.

Table 3 Stern–Volmer constants K_{SV} and binding constants K_{app} towards CT-DNA for **Ag(L4)**, **Ag(L5)**, and $AgNO_3$

Compound	K_{SV} [M^{-1}]	K_{app} [M^{-1}]
Ag(L4)	0.44×10^3	0.57×10^4
Ag(L5)	0.67×10^3	0.87×10^4
$AgNO_3$	1.98×10^5	2.57×10^6

Conclusions

Five new homoleptic Ag(I) DTC complexes with ligands derived from amino acid esters were synthesised and extensively characterised by different analytical techniques, including spectroscopic methods, as well as computational modelling. TGA showcases that their thermal stability is in the same range as for unsubstituted Ag DTCs.[49,50,53,55,57–60,71] Single-crystal X-ray structural analysis showed the presence of rather complex coordination polymers in the solid state, comprising ribbon-like polymeric assemblies for both **Ag(L4)** and **Ag(L5)**, while the structure of **Ag(L1)** shows dimeric and hexameric subunits, that alternate to form a one-dimensional polymer as well. By contrast, the results of DOSY NMR studies and DFT calculations point toward the presence of smaller aggregates like dimers, tetramers, and possibly hexamers in solution. These results show that the structural chemistry of Ag(I) AA-DTCs is basically different from that of multiply charged transition metal ions, showing a much fewer tendency (Cu(II)[85]) or even no tendency (Ni(II), Pd(II), Pt(II)[86,87]) toward aggregation into coordination oligomers and polymers. It can be presumed that a similar behaviour as for Ag(I) can be expected for other monovalent metal centres such as Cu(I) and Au(I). Initial biological evaluations of the silver compounds comprising EB displacement assays and DNA melting curve experiments carried out for **Ag(L4)** and **Ag(L5)** revealed moderate DNA binding abilities.

The products reported herein expand the scope of Ag(I) DTC compounds towards carboxylic-ester functionalised ligands. These additional functional groups can not only impact characteristics like solubility, stability and biological activity, but could also allow the coordination of a second metal upon cleavage of the ester group. This could result in the formation of heterobimetallic networks with a second metal connecting the polymeric strands of these homometallic silver compounds. Ag(I) DTC compounds with free carboxylate functional groups and their bimetallic derivatives are the objective of our ongoing research.

Experimental

General

Unless otherwise noted, all operations were performed under atmospheric conditions without exclusion of air. All starting materials were obtained from commercial suppliers and used without further purification. IR spectra were measured on a Bruker Vertex 70 FTIR spectrometer equipped with a diamond ATR unit and ESI mass spectra on a Thermo LTQ machine (solvent: methanol). Elemental analyses were performed using a HEKAtech Eurovector EA3000 CHNS analyzer. Thermal analyses (TGA) were performed using a Netzsch STA 449 F1 Jupiter thermobalance. The samples were measured in a temperature range from room temperature to 600 °C with a heating rate of 10 K min^{-1} under nitrogen. The X-ray crystallographic data were collected on a Bruker-Nonius Kappa-CCD diffractometer at 120 K and are summarized in Table S5 in the SI. The crystal structures were solved with SHELXT-2018/3 [88] and refined by full matrix least-squares methods on F^2 with SHELXL-2018/3,[89] using the Olex2 1.5 environment.[90] Multi-scan absorption correction was applied to the intensity data.[91] The geometric environment of the silver atoms was analysed on the basis of continuous symmetry measures using SHAPE 2.1.[74]

NMR spectroscopy

NMR spectra were recorded on a Bruker Avance III (^{1}H: 400.13 MHz, ^{13}C: 100.6 MHz) with a 5 mm PA BBO 400S1 BBF-H-D-05 Z probehead, Bruker Avance NEO 500 (^{1}H: 500.18 MHz, ^{13}C: 125.7 MHz) with a CPP BBFO Prodigy probehead or Bruker Avance III 600 (^{1}H: 600.15 MHz, ^{13}C: 150.9 MHz) with a 5 mm QCI CP2 cryoprobe at ambient temperature. ^{1}H and ^{13}C shifts are referenced to tetramethylsilane (δ = 0 ppm). ^{1}H DOSY NMR spectra were acquired at 297 K in a Bruker Avance NEO 500 (500.18 MHz, ^{1}H; 125.7 MHz, ^{13}C) spectrometer equipped with a broadband cryoprobehead (Prodigy). The double stimulated echo sequence with bipolar gradient pulses and three spoil gradients with convection compensation from Bruker (dstebpgp3s) was used. The diffusion time was 50–100 ms and the duration of the magnetic field pulse gradients 2–4 ms. The delay for gradient recovery was 0.2 ms and the eddy current delay 5 ms. For each experiment, a series of 32 spectra on 32 K data points were collected. After Fourier transformation and baseline correction, the diffusion dimension was processed with the Topspin 4.4 software and the diffusion coefficients were calculated by Gaussian fits with the relaxation $T1/T2$ software of Topspin.

Computational details

All DFT calculations were carried out with the quantum chemistry package Gaussian 16.[92] DFT was used to optimise the singlet equilibrium geometry and to gather thermodynamical properties of the Ag complexes of interest. If not stated otherwise the hybrid functional B3LYP[93] in combination with the triple-ζ basis set def2-TZVP[94] was used in combination with D3BJ dispersion correction.[95] Implicit solvent effects were taken into account (acetonitrile and chloroform) by means of an implicit solvation model (SMD).[96] To verify if a (local) minimum of the potential energy surface was found and to obtain thermodynamical properties such as Gibbs energy, a harmonic frequency calculation at 298.15 K was performed afterwards, where no imaginary frequencies were found. All molecular orbitals were visualised utilising MultiWFN[97] and plotting them with UCSF Chimera, developed by the Resource for Biocomputing, Visualization, and Informatics at the University of California, San Francisco, with support from NIH P41-GM103311.[98] In particular, the following oligomers, based on the dimer $[Ag(L2)]_2$, and their formation were investigated by quantum chemical simulations:

$$[Ag(L2)]_2 \rightarrow \frac{1}{2}[Ag(L2)]_4 \quad (1)$$

$$[Ag(L2)]_2 + 2MeCN \rightarrow 2[Ag(L2)MeCN] \quad (2)$$

$$[Ag(L2)]_2 + 2MeCN \rightarrow [Ag(MeCN)_2]^+ + [Ag(L2)_2]^-. \quad (3)$$

Ethidium bromide (EB) displacement assay

Stock solutions for each compound were prepared to 10 mM in DMSO. A diluted solution to 5 mM in DMSO was used for the titration steps. A mixture of calf thymus (CT) DNA (20 μM) and EB (1.3 μM) in HEPES buffer (50 mM, pH 7.4) was prepared in a 1 mL fluorescence cuvette. After 15 min, this solution was treated with increasing amounts of the Ag complexes **Ag(L4)**, **Ag(L5)** (0 → 100 μM) or $AgNO_3$ (0 → 5 μM). Due to titration the DMSO amount in the experiment increased from 0 up to 2%. The fluorescence spectra were collected after each addition, mixing and a waiting time of 1 min in a range of 550–700 nm using an excitation wavelength of 518 nm on a HORIBA FluoroMax®-3 with excitation and emission slit of 5 nm.

DNA melting curves

DNA melting curves of CT-DNA (50 μM) in HEPES buffer (50 mM, pH 7.4) in the presence of the **Ag(L4)**, **Ag(L5)** or $AgNO_3$ (2.5 μM) were measured at 260 nm in 1% DMSO. The temperature range was 65–95 °C and a heating rate of 0.5 °C min^{-1} was used. The measurement interval was 1 °C. Before the measurement the temperature was held constant for 1 min. Five Hellma cuvettes with 1 mL sample volume each were used for carrying out the experiment simultaneously. Normalization of melting curves was utilized for better visualization.

General synthetic procedure of complexes Ag(L1)–Ag(L5)

To an ice-cooled solution of the amino acid ester (4 equiv.) in water (5 mL), CS_2 (2 equiv.) was added under vigorous stirring. In case of an amino acid ester hydrochloride, KOH (0.5 mol L^{-1}, 4 equiv.) was added to the initial solution. After stirring for 1–2 h, a solution of $AgNO_3$ (1 equiv.) in water (2 mL) was added to the reaction mixture. Stirring was continued for 30 min at room temperature, before the precipitated product was isolated by vacuum filtration or centrifugation, washed with water and dried in a desiccator over silica or H_2SO_4.

$[Ag\{SSC\text{-}N(CH_2COOEt)_2\}]_n$ (Ag(L1)). **Ag(L1)** was prepared using iminodiacetic acid diethyl ester (0.37 mL, 390 mg, 2 mmol) in water (5 mL), CS_2 (0.06 mL, 1 mmol) and $AgNO_3$ (85 mg, 0.5 mmol) in water (2 mL). Yield: 145 mg (78%). The pale yellow powdery solid was insoluble in water, isopropanol, ethanol and diethyl ether, moderately soluble in methanol and chloroform and soluble in DMSO and acetonitrile. Dec. 227 °C. Anal. calcd for $C_9H_{14}AgNO_4S_2$ (M = 372.2 g mol^{-1}): C 29.0, H 3.8, N 3.8%. Found: C 28.3, H 3.6, N 4.2%. ^{1}H NMR (DMSO-d$_6$): δ 4.87 (s, 4H, CH_2), 4.15 (q, $^3J_{H,H}$ = 3 × 7.1 Hz, 4H, CH_2), 1.22 (t, $^3J_{H,H}$ = 2 × 7.1 Hz, 6H; CH_3) ppm. ^{13}C NMR (DMSO-d$_6$): δ 208.4 (*C*SS), 167.3 (*C*OOEt), 61.7 (CH_2), 59.6 (CH_2), 14.6 (CH_3) ppm. ESI(+)-MS: m/z 190.1 (12%, [M – CSSAg + 2H]$^+$), 1223.9 (50%; [4M − L]$^+$), 1596.7 (99%; [5M − L]$^+$), 1967.3 (100%; [6M − L]$^+$). IR: $\tilde{\nu}$ 2986wbr, 1728s, 1466m, 1414sh, 1391m, 1371m, 1337m, 1296m, 1261w, 1196s, 1165s, 1098w, 1011s, 986s, 947s, 926sh, 866w, 849w, 737w, 544m, 436m, 330m cm^{-1}. Single-crystals suitable for X-ray structural analysis were obtained from water/ethanol.

$[Ag\{SSC\text{-}N(CH_3)(CH_2COOEt)\}]_n$ (Ag(L2)). **Ag(L2)** was prepared using sarcosine ethyl ester hydrochloride (317 mg, 2 mmol) and KOH (4 mL, 0.5 mol L^{-1}, 2 mmol) in a total volume of 5 ml water, CS_2 (0.06 mL, 1 mmol) and $AgNO_3$ (85 mg, 0.5 mmol) in water (2 mL). Yield: 149 mg (99%). The pale yellow powdery solid was insoluble in water and organic solvents such as acetone, acetonitrile, chloroform, dichloromethane, DMSO, methanol, and pyridine. Dec. 236 °C. Anal. calcd for $C_6H_{10}AgNO_2S_2$ (M = 300.14 g mol^{-1}): C 24.0, H 3.4, N 4.7%. Found: C 23.6, H 3.3, N 4.4%. IR: $\tilde{\nu}$ 2928br, 1730s, 1470m, 1443w, 1400w, 1371m, 1350w, 1269sh, 1250m, 1198s, 1090m, 1024m, 1003m, 964s, 936w, 899w, 853m, 808w, 787w, 613m, 557m, 482m, 432w, 343w cm^{-1}.

$[Ag\{SSC\text{-}N(CH_3)(CH_2COO\textit{t}Bu)\}]_n$ (Ag(L3)). **Ag(L3)** was prepared using sarcosine *tert*-butyl ester hydrochloride (363 mg, 2 mmol) and KOH (4 mL, 0.5 mol L^{-1}, 2 mmol) in a total volume of 5 mL water, CS_2 (0.06 mL, 1 mmol) and $AgNO_3$ (85 mg, 0.5 mmol) in water (2 mL). Yield: 160 mg (98%). The pale yellow powdery solid was soluble in chloroform and dichloromethane, poorly soluble in DMSO and acetonitrile and insoluble in water and most other organic solvents. Dec. 199 °C. Anal. calcd for $C_8H_{14}AgNO_2S_2$ (M = 328.19 g mol^{-1}): C 29.3, H 4.3, N 4.3%. Found: C 29.0, H 4.3, N 4.4%. ^{1}H NMR ($CDCl_3$): δ 4.73 (s, 2H, CH_2), 3.63 (s, 3H, CH_3), 1.51 (s, 9H, $3CH_3$) ppm. ^{13}C NMR ($CDCl_3$): δ 207.9 (*C*SS), 166.5 (*C*OO*t*Bu), 82.5 (*C*), 61.1 (CH_2), 46.8 (CH_3), 28.2 (CH_3) ppm. ESI(+)-MS: m/z 1091.8 (28%; [4M − L]$^+$), 1420.7 (73%; [5M − L]$^+$), 1747.4 (100%; [6M − L]$^+$). IR: $\tilde{\nu}$ 2980br, 2932br, 1734s, 1476m, 1366m, 1356m, 1283w, 1269w, 1211m, 1153s, 1088m, 1005w, 970s, 945w, 903w, 847w, 752w, 737w, 571w, 554w, 502w, 438m, 363w, 326w cm^{-1}.

$[Ag(SSC\text{-}NC_4H_7COOMe)]_n$ (Ag(L4)). **Ag(L4)** was prepared using L-proline methyl ester hydrochloride (338 mg, 2 mmol) and KOH (4 mL, 0.5 mol L^{-1}, 2 mmol) in a total volume of 5 mL water, CS_2 (0.06 mL, 1 mmol) and $AgNO_3$ (85 mg, 0.5 mmol) in water (2 mL). Yield: 155 mg (99%). The pale yellow powdery solid was insoluble in water, acetone, methanol and diethyl ether, and soluble in DMSO, chloroform, and acetonitrile. Dec. 240 °C. Anal. calcd for $C_7H_{10}AgNO_2S_2$ (M = 312.15 g mol^{-1}): C 26.9, H 3.2, N 4.5%. Found: C 26.5, H 3.2, N 4.5%. ^{1}H NMR ($CDCl_3$): δ 5.13–5.10 (m, 1H, C*H*), 4.13–3.95 (m, 2H, CH_2), 3.77 (s, 3H, CH_3), 2.49–2.39 (m, 1H), 2.19–2.06 (m, 3H) ppm. ^{13}C NMR ($CDCl_3$): δ 203.2 (*C*SS), 171.2 (*C*OOMe), 67.8 (*C*H), 56.8 (CH_2), 52.6 (CH_3), 31.6 (CH_2), 25.0 (CH_2) ppm. ESI(+)-MS: m/z 1043.7 (23%; [4M − L]$^+$), 1354.6 (70%; [5M − L]$^+$), 1667.2 (100%; [6M − L]$^+$), 1979.8 (85%; [7M − L]$^+$). IR: $\tilde{\nu}$ 2949wbr, 1740s, 1730s, 1452sh, 1414s, 1358m, 1333m, 1265m, 1234w, 1200m, 1165s, 1152s, 1086m, 1044w, 999m, 988sh, 934s, 895w, 876w, 839w, 773m, 729w, 681m, 606w, 588w, 563w, 482w, 451m, 357m cm^{-1}. Single-crystals suitable for X-ray structural analysis were obtained from a solution in DMSO.

$[Ag\{SSC\text{-}N(CH_2Ph)(CH_2COOEt)\}]_n$ (Ag(L5)). To an ice-cooled solution of *N*-benzyl glycine ethyl ester (0.4 mL, 2 mmol) in methanol (5 mL) CS_2 (0.06 mL, 1 mmol) was added under vigorous stirring. After stirring for 1 h, a solution of $AgNO_3$ (85 mg, 0.5 mmol) in DMSO (10 mL) was added dropwise at room temperature. The resulting clear yellow solution was layered with methanol which led to the formation of needle like crystals within two weeks, which were suitable for X-ray diffraction analysis. The crystalline product was isolated by vacuum filtration, washed with diethyl ether, and dried under air. Yield: 175 mg (93%). The yellow crystalline solid was insoluble in water, acetone, methanol and diethyl ether, and soluble in DMSO, chloroform, and acetonitrile. Dec. 251 °C. Anal. calcd for $C_{12}H_{14}AgNO_2S_2$ (M = 376.24 g mol^{-1}): C 38.3, H 3.8, N 3.7%. Found: C 38.5, H 3.7, N 3.7%. ^{1}H NMR (DMSO-d$_6$): δ 7.39 (d, $^3J_{H,H}$ = 7.31 Hz, 2H, Ar*H*), 7.33–7.23 (m, 3H, Ar*H*), 5.37 (s, 2H, CH_2), 4.66 (s, 2H, CH_2), 4.09 (q, $^3J_{H,H}$ = 7.02 Hz, 2H, $COOCH_2$), 1.16 (t, $^3J_{H,H}$ = 7.16 Hz, 3H, CH_3) ppm. ^{13}C NMR (DMSO-d$_6$): δ 208.4 (*C*SS), 167.4 (*C*OOEt), 135.6 (*C*), 128.9 (2*C*H), 128.2 (2*C*H), 128.0 (*C*H), 61.4 ($2CH_2$), 57.5 (CH_2), 14.5 (CH_3) ppm. ESI(+)-MS: m/z 194.1 (100%; [M – CSSAg + 2H]$^+$), 1987.4 (5%, [6M − L]$^+$). IR: $\tilde{\nu}$ 2976w, 2930wbr, 1734s, 1603w, 1497w, 1454m, 1427m, 1416m, 1387m, 1371sh, 1342w, 1331w, 1296w, 1271m, 1246m, 1213m, 1182s, 1159s, 1096w, 1080w, 1024m, 1001s, 974s, 939s, 901sh, 853w, 810w, 787w, 737m, 719w, 698s, 681m, 644w, 590m, 569m, 544m, 521m, 455w, 430w, 409w, 355m cm^{-1}.

Author contributions

V. B.: conceptualisation, data curation, formal analysis, investigation, methodology, supervision, validation, visualisation, writing – original draft; Ja. H.: data curation, formal analysis, investigation; D. D.: data curation, formal analysis, investigation, validation, software, writing – review and editing; E. P. B.: data curation, formal analysis, investigation, software; Ju. H.: conceptualization, data curation, formal analysis, investigation, methodology, validation; N. S.: methodology, supervision, writing – review and editing; S. K.: methodology, supervision, writing – review and editing; N. K.: methodology, supervision, writing – review and editing; P. K.: conceptualization,

funding acquisition, methodology, project administration, supervision, validation, writing – review and editing.

Conflicts of interest

There are no conflicts to declare.

Data availability

All fully relaxed structures are freely available *via* the online repository Zenodo (**https://doi.org/10.5281/zenodo.15699345**).

Supplementary information is available: IR, NMR, and ESI mass spectra, TGA diagrams, details on DOSY NMR study, DFT calculations, DNA interaction studies, and single-crystal X-ray structural analyses. See DOI: **https://doi.org/10.1039/d5dt01476j**.

CCDC 2463483, 2440220 and 2440221 contains the supplementary crystallographic data for this paper.[99a–c]

Acknowledgements

This work is supported by the German Research Foundation (DFG), project number 462687456 (**https://gepris.dfg.de/gepris/projekt/462687456**). Acquisition of the 500 MHz NMR spectrometer was supported by a grant 'Forschungsgroßgeräte nach Art. 91b', grant INST 275/442-1 FUGG of the DFG. General financial support of the Friedrich Schiller University Jena is gratefully acknowledged.

References

1 P. Köhler, *Eur. J. Inorg. Chem.*, 2025, **28**, e202500007.
2 S. H. Crook, B. E. Mann, A. J. H. M. Meijer, H. Adams, P. Sawle, D. Scapens and R. Motterlini, *Dalton Trans.*, 2011, **40**, 4230–4235.
3 X. Wang, B. Gao, G. Sebit Ahmed Suleiman, X.-k. Ren, J. Guo, S. Xia, W. Zhang and Y. Feng, *Chem. Eng. J.*, 2021, **424**, 130430.
4 L. Wu, X. Cai, H. Zhu, J. Li, D. Shi, D. Su, D. Yue and Z. Gu, *Adv. Funct. Mater.*, 2018, **28**, 1804324.
5 T. Zhang, M. Li, Y. Gong, N. Xi, Y. Zheng, Q. Zhao, Y. Chen and B. Liu, *JBIC, J. Biol. Inorg. Chem.*, 2016, **21**, 807–824.
6 Y. Chen, H. Guo, F. Xie and J. Lu, *J. Labelled Compd. Radiopharm.*, 2014, **57**, 12–17.
7 M. Liu, X. Lin, X. Song, Y. Cui, P. Li, X. Wang and J. Zhang, *J. Radioanal. Nucl. Chem.*, 2013, **298**, 1659–1663.
8 M. A. Stalteri, S. J. Parrott, V. A. Griffiths, J. R. Dilworth and S. J. Mather, *Nucl. Med. Commun.*, 1997, **18**, 870–877.
9 S. Fujii, Y. Suzuki, T. Yoshimura and H. Kamada, *Am. J. Physiol.*, 1998, **274**, G857–G862.
10 S. Fujii, K. Kobayashi, S. Tagawa and T. Yoshimura, *J. Chem. Soc., Dalton Trans.*, 2000, 3310–3315.
11 H. Nakagawa, N. Ikota, T. Ozawa, T. Masumizu and M. Kohno, *Biochem. Mol. Biol. Int.*, 1998, **45**, 1129–1138.
12 S. Pou, P. Tsai, S. Porasuphatana, H. J. Halpern, G. V. Chandramouli, E. D. Barth and G. M. Rosen, *Biochim. Biophys. Acta*, 1999, **1427**, 216–226.
13 H. Yasui, S. Fujii, T. Yoshimura and H. Sakurai, *Free Radical Res.*, 2004, **38**, 1061–1072.
14 L. Brustolin, C. Nardon, N. Pettenuzzo, N. Zuin Fantoni, S. Quarta, F. Chiara, A. Gambalunga, A. Trevisan, L. Marchiò, P. Pontisso and D. Fregona, *Dalton Trans.*, 2018, **47**, 15477–15486.
15 C. Chen, K.-W. Yang, Le Zhai, H.-H. Ding and J.-Z. Chigan, *Bioorg. Chem.*, 2022, **118**, 105474.
16 A. M. Díaz, R. Villalonga and R. Cao, *J. Coord. Chem.*, 2009, **62**, 100–107.
17 L. Giovagnini, S. Sitran, M. Montopoli, L. Caparrotta, M. Corsini, C. Rosani, P. Zanello, Q. P. Dou and D. Fregona, *Inorg. Chem.*, 2008, **47**, 6336–6343.
18 D. Aldinucci, L. Cattaruzza, D. Lorenzon, L. Giovagnini, D. Fregona and A. Colombatti, *Oncol. Res.*, 2008, **17**, 103–113.
19 V. Alverdi, L. Giovagnini, C. Marzano, R. Seraglia, F. Bettio, S. Sitran, R. Graziani and D. Fregona, *J. Inorg. Biochem.*, 2004, **98**, 1117–1128.
20 G. Faraglia, D. Fregona, S. Sitran, L. Giovagnini, C. Marzano, F. Baccichetti, U. Casellato and R. Graziani, *J. Inorg. Biochem.*, 2001, **83**, 31–40.
21 L. Giovagnini, L. Ronconi, D. Aldinucci, D. Lorenzon, S. Sitran and D. Fregona, *J. Med. Chem.*, 2005, **48**, 1588–1595.
22 M. P. Kasalović, A. Petrović, J. M. Živković, L. Kuckling, V. V. Jevtić, J. Bogojeski, Z. B. Leka, S. R. Trifunović and N. Đ. Pantelić, *J. Mol. Struct.*, 2021, **1229**, 129622.
23 L. Sindellari, L. Trincia, M. Nicolini, M. Carrara, L. Cima and S. Zampiron, *Inorg. Chim. Acta*, 1987, **137**, 109–113.
24 A. Trevisan, C. Marzano, P. Cristofori, M. Borella Venturini, L. Giovagnini and D. Fregona, *Arch. Toxicol.*, 2002, **76**, 262–268.
25 C. Marzano, F. Bettio, F. Baccichetti, A. Trevisan, L. Giovagnini and D. Fregona, *Chem.-Biol. Interact.*, 2004, **148**, 37–48.
26 R. Verron, T. Achard, C. Seguin, S. Fournel and S. Bellemin-Laponnaz, *Eur. J. Inorg. Chem.*, 2020, **2020**, 2552–2557.
27 D. Aldinucci, D. Lorenzon, L. Stefani, L. Giovagnini, A. Colombatti and D. Fregona, *Anti-Cancer Drugs*, 2007, **18**, 323–332.
28 G. Boscutti, C. Nardon, L. Marchiò, M. Crisma, B. Biondi, D. Dalzoppo, L. Dalla Via, F. Formaggio, A. Casini and D. Fregona, *ChemMedChem*, 2018, **13**, 1131–1145.
29 A. K. Hartmann, S. Gudipati, A. Pettenuzzo, L. Ronconi and J. L. Rouge, *Bioconjugate Chem.*, 2020, **31**, 1063–1069.
30 C. Marzano, L. Ronconi, F. Chiara, M. C. Giron, I. Faustinelli, P. Cristofori, A. Trevisan and D. Fregona, *Int. J. Cancer*, 2011, **129**, 487–496.
31 C. Nardon, G. Boscutti, C. Gabbiani, L. Massai, N. Pettenuzzo, A. Fassina, L. Messori and D. Fregona, *Eur. J. Inorg. Chem.*, 2017, **2017**, 1737–1744.

32 L. Ronconi, L. Giovagnini, C. Marzano, F. Bettìo, R. Graziani, G. Pilloni and D. Fregona, *Inorg. Chem.*, 2005, **44**, 1867–1881.
33 L. Ronconi, C. Marzano, P. Zanello, M. Corsini, G. Miolo, C. Maccà, A. Trevisan and D. Fregona, *J. Med. Chem.*, 2006, **49**, 1648–1657.
34 L. Giovagnini, S. Sitran, I. Castagliuolo, P. Brun, M. Corsini, P. Zanello, A. Zoleo, A. Maniero, B. Biondi and D. Fregona, *Dalton Trans.*, 2008, 6699–6708.
35 E. M. Nagy, C. Nardon, L. Giovagnini, L. Marchiò, A. Trevisan and D. Fregona, *Dalton Trans.*, 2011, **40**, 11885–11895.
36 A.-C. Burduşel, O. Gherasim, A. M. Grumezescu, L. Mogoantč, A. Ficai and E. Andronescu, *Nanomaterials*, 2018, **8**, 681.
37 S. Medici, M. Peana, G. Crisponi, V. M. Nurchi, J. I. Lachowicz, M. Remelli and M. A. Zoroddu, *Coord. Chem. Rev.*, 2016, **327–328**, 349–359.
38 G. Hogarth, *Progress in Inorganic Chemistry*, John Wiley & Sons, Ltd, 2005, pp. 71–561.
39 R. Hesse, L. Nilson, C. Larsen, P. H. Nielsen, A. A. Lindberg, G. Jansen, B. Lamm and B. Samuelsson, *Acta Chem. Scand.*, 1969, **23**, 825–845.
40 W. Su, M. Hong, F. Jiang, H. Liu, Z. Zhou, D. Wu and T. Mak, *Polyhedron*, 1996, **15**, 4047–4051.
41 H. Yamaguchi, A. Kido, T. Uechi and K. Yasukouchi, *Bull. Chem. Soc. Jpn.*, 1976, **49**, 1271–1276.
42 X. Yin, M.-B. Xie, W.-G. Zhang, J. Fan and M. Zeller, *Acta Crystallogr., Sect. E: Struct. Rep. Online*, 2007, **63**, m2063–m2064.
43 S. D. Oladipo and B. Omondi, *Molbank*, 2022, **2022**, M1327.
44 H. Anacker-Eickhoff, R. Hesse, P. Jennische, A. Wahlberg, O. Bastiansen, G. Braathen, L. Fernholt, G. Gundersen, C. J. Nielsen, B. N. Cyvin and S. J. Cyvin, *Acta Chem. Scand.*, 1982, **36a**, 251–258.
45 N. Masciocchi, S. Brenna, S. Galli and A. Maspero, *Z. Kristallogr. – Cryst. Mater.*, 2003, **218**, 450–454.
46 Y.-W. Song, Z. Yu and Q.-F. Zhang, *Acta Crystallogr., Sect. C: Cryst. Struct. Commun.*, 2006, **C62**, m214–m216.
47 X. Yin, M.-B. Xie, W.-G. Zhang and J. Fan, *Acta Crystallogr., Sect. E: Struct. Rep. Online*, 2007, **63**, m2273–m2273.
48 D.-J. Zhang, S.-Y. Yang and B. K. Teo, *J. Cluster Sci.*, 2017, **28**, 1163–1178.
49 U. K. Chaudhari, A. Bharti, P. Nath, U. P. Azad, R. Prakash, R. J. Butcher and M. K. Bharty, *J. Mol. Struct.*, 2019, **1177**, 260–268.
50 R. Mothes, A. Jakob, T. Waechtler, S. E. Schulz, T. Gessner and H. Lang, *Eur. J. Inorg. Chem.*, 2015, **2015**, 1726–1733.
51 S. D. Oladipo, G. F. Tolufashe, C. Mocktar and B. Omondi, *Inorg. Chim. Acta*, 2021, **520**, 120316.
52 C. Di Nicola, J. Ngoune, Effendy, C. Pettinari, B. W. Skelton and A. H. White, *Inorg. Chim. Acta*, 2007, **360**, 2935–2943.
53 P. Nath, M. K. Bharty, B. Maiti, A. Bharti, R. J. Butcher, J. L. Wikaira and N. K. Singh, *RSC Adv.*, 2016, **6**, 93867–93880.
54 Y. J. Tan, Y. S. Tan, C. I. Yeo, J. Chew and E. R. T. Tiekink, *J. Inorg. Biochem.*, 2019, **192**, 107–118.
55 V. Kumar, V. Singh, A. N. Gupta, K. K. Manar, L. B. Prasad, M. G. B. Drew and N. Singh, *New J. Chem.*, 2014, **38**, 4478–4485.
56 P. A. Ajibade, T. B. Mbuyazi and A. M. Paca, *ACS Omega*, 2023, **8**, 24750–24760.
57 E. V. Korneeva, A. I. Smolentsev, O. N. Antzutkin and A. V. Ivanov, *Inorg. Chim. Acta*, 2021, **525**, 120383.
58 G. Rajput, M. K. Yadav, M. G. B. Drew and N. Singh, *Inorg. Chem.*, 2015, **54**, 2572–2579.
59 B.-C. Tzeng, C.-L. Wu, J.-W. Hung, S.-Y. Chien and G.-H. Lee, *Dalton Trans.*, 2022, **51**, 16973–16981.
60 R. H. K. Varma and C. P. Prabhakaran, *Indian J. Chem., Sect. A*, 1989, **28**, 1119–1121.
61 G. Boscutti, L. Feltrin, D. Lorenzon, S. Sitran, D. Aldinucci, L. Ronconi and D. Fregona, *Inorg. Chim. Acta*, 2012, **393**, 304–317.
62 G. Boscutti, L. Marchiò, L. Ronconi and D. Fregona, *Chem. – Eur. J.*, 2013, **19**, 13428–13436.
63 L. Cattaruzza, D. Fregona, M. Mongiat, L. Ronconi, A. Fassina, A. Colombatti and D. Aldinucci, *Int. J. Cancer*, 2011, **128**, 206–215.
64 M. N. Kouodom, G. Boscutti, M. Celegato, M. Crisma, S. Sitran, D. Aldinucci, F. Formaggio, L. Ronconi and D. Fregona, *J. Inorg. Biochem.*, 2012, **117**, 248–260.
65 X. Zhang, M. Frezza, V. Milacic, L. Ronconi, Y. Fan, C. Bi, D. Fregona and Q. P. Dou, *J. Cell. Biochem.*, 2010, **109**, 162–172.
66 E. Pretsch, P. Bühlmann and M. Badertscher, *Spektroskopische Daten zur Strukturaufklärung organischer Verbindungen*, Springer Spektrum, Berlin, 2020, pp. 307–373.
67 E. Pretsch, P. Bühlmann and M. Badertscher, *Spektroskopische Daten zur Strukturaufklärung organischer Verbindungen*, Springer Spektrum, Berlin, 2020, pp. 75–165.
68 L. I. Victoriano and H. B. Cortés, *J. Coord. Chem.*, 1996, **39**, 231–239.
69 W. Beck, M. Girnth, M. Castillo and H. Zippel, *Chem. Ber.*, 1978, **111**, 1246–1252.
70 E. M. Nagy, S. Sitran, M. Montopoli, M. Favaro, L. Marchiò, L. Caparrotta and D. Fregona, *J. Inorg. Biochem.*, 2012, **117**, 131–139.
71 R. Mothes, H. Petzold, A. Jakob, T. Rüffer and H. Lang, *Inorg. Chim. Acta*, 2015, **429**, 227–236.
72 F. H. Allen, O. Kennard, D. G. Watson, L. Brammer, A. G. Orpen and R. Taylor, *J. Chem. Soc., Perkin Trans. 2*, 1987, S1.
73 C. R. Groom, I. J. Bruno, M. P. Lightfoot and S. C. Ward, *Acta Crystallogr., Sect. B: Struct. Sci., Cryst. Eng. Mater.*, 2016, **72**, 171–179.
74 M. Pinsky and D. Avnir, *Inorg. Chem.*, 1998, **37**, 5575–5582.
75 D. Li, G. Kagan, R. Hopson and P. G. Williard, *J. Am. Chem. Soc.*, 2009, **131**, 5627–5634.
76 E. H. P. Brohmer and S. Kupfer, *Silver Dithiocarbamates Derived from Amino Acid Esters*, 2025, DOI: DOI: **10.5281/zenodo.15699345**.

77 S. Roy, A. K. Patra, S. Dhar and A. R. Chakravarty, *Inorg. Chem.*, 2008, **47**, 5625–5633.
78 X. Sheng, X.-M. Lu, Y.-T. Chen, G.-Y. Lu, J.-J. Zhang, Y. Shao, F. Liu and Q. Xu, *Chem. – Eur. J.*, 2007, **13**, 9703–9712.
79 J. Heinrich, K. Bossak-Ahmad, M. Riisom, H. H. Haeri, T. R. Steel, V. Hergl, A. Langhans, C. Schattschneider, J. Barrera, S. M. F. Jamieson, M. Stein, D. Hinderberger, C. G. Hartinger, W. Bal and N. Kulak, *Chem. – Eur. J.*, 2021, **27**, 18093–18102.
80 A. Ono, S. Cao, H. Togashi, M. Tashiro, T. Fujimoto, T. Machinami, S. Oda, Y. Miyake, I. Okamoto and Y. Tanaka, *Chem. Commun.*, 2008, 4825–4827.
81 S. M. Swasey, L. E. Leal, O. Lopez-Acevedo, J. Pavlovich and E. G. Gwinn, *Sci. Rep.*, 2015, **5**, 10163.
82 S. Mandal, A. Hepp and J. Müller, *Dalton Trans.*, 2015, **44**, 3540–3543.
83 I. Sinha, C. Fonseca Guerra and J. Müller, *Angew. Chem., Int. Ed.*, 2015, **54**, 3603–3606.
84 B. Jash and J. Müller, *Chem. – Eur. J.*, 2018, **24**, 10636–10640.
85 V. Behling, B. Kintzel, J. Heinrich, M. Hingel, J. Meyer, S. Greiner and P. Liebing, *Cryst. Growth Des.*, 2023, **23**, 7777–7788.
86 P. Liebing, F. Oehler and J. Witzorke, *Crystals*, 2020, **10**, 505.
87 P. Liebing, J. Witzorke, F. Oehler and M. Schmeide, *Inorg. Chem.*, 2020, **59**, 2825–2832.
88 G. M. Sheldrick, *Acta Crystallogr., Sect. C: Cryst. Struct. Commun.*, 2015, **71**, 3–8.
89 G. M. Sheldrick, *Acta Crystallogr., Sect. A: Found. Adv.*, 2015, **71**, 3–8.
90 O. V. Dolomanov, L. J. Bourhis, R. J. Gildea, J. A. K. Howard and H. Puschmann, *J. Appl. Crystallogr.*, 2009, **42**, 339–341.
91 *Bruker AXS, Apex5 and SADABS*, 2001.
92 M. J. Frisch, G. W. Trucks, H. B. Schlegel, G. E. Scuseria, M. A. Robb, J. R. Cheeseman, G. Scalmani, V. Barone, G. A. Petersson, H. Nakatsuji, X. Li, M. Caricato, A. V. Marenich, J. Bloino, B. G. Janesko, R. Gomperts, B. Mennucci, H. P. Hratchian, J. V. Ortiz, A. F. Izmaylov, J. L. Sonnenberg, D. Williams-Young, F. Ding, F. Lipparini, F. Egidi, J. Goings, B. Peng, A. Petrone, T. Henderson, D. Ranasinghe, V. G. Zakrzewski, J. Gao, N. Rega, G. Zheng, W. Liang, M. Hada, M. Ehara, K. Toyota, R. Fukuda, J. Hasegawa, M. Ishida, T. Nakajima, Y. Honda, O. Kitao, H. Nakai, T. Vreven, K. Throssell, J. A. Montgomery Jr., J. E. Peralta, F. Ogliaro, M. J. Bearpark, J. J. Heyd, E. N. Brothers, K. N. Kudin, V. N. Staroverov, T. A. Keith, R. Kobayashi, J. Normand, K. Raghavachari, A. P. Rendell, J. C. Burant, S. S. Iyengar, J. Tomasi, M. Cossi, J. M. Millam, M. Klene, C. Adamo, R. Cammi, J. W. Ochterski, R. L. Martin, K. Morokuma, O. Farkas, J. B. Foresman and D. J. Fox, *Gaussian 16, Revision C.01*, 2016.
93 S. Grimme, J. Antony, S. Ehrlich and H. Krieg, *J. Chem. Phys.*, 2010, **132**, 154104.
94 A. Hellweg and D. Rappoport, *Phys. Chem. Chem. Phys.*, 2015, **17**, 1010–1017.
95 S. Grimme, S. Ehrlich and L. Goerigk, *J. Comput. Chem.*, 2011, **32**, 1456–1465.
96 A. V. Marenich, C. J. Cramer and D. G. Truhlar, *J. Phys. Chem. B*, 2009, **113**, 6378–6396.
97 T. Lu, *J. Chem. Phys.*, 2024, **161**, 082503.
98 E. F. Pettersen, T. D. Goddard, C. C. Huang, G. S. Couch, D. M. Greenblatt, E. C. Meng and T. E. Ferrin, *J. Comput. Chem.*, 2004, **25**, 1605–1612.
99 (*a*) V. Behling and P. Köhler, CCDC 2463483 (**Ag(L1)**): Experimental Crystal Structure Determination, 2025, DOI: **10.5517/ccdc.csd.cc2npg61**; (*b*) V. Behling, J. Heinrich and P. Köhler, CCDC 2440220 (**Ag(L4)**): Experimental Crystal Structure Determination, 2025, DOI: **10.5517/ccdc.csd.cc2mx7sl**; (*c*) V. Behling, J. Heinrich and P. Köhler, CCDC 2440221 (**Ag(L5)**): Experimental Crystal Structure Determination, 2025, DOI: **10.5517/ccdc.csd.cc2mx7tm**.